Hindawi
Geofluids
Volume 2023, Article ID 7360208, 9 pages
https://doi.org/10.1155/2023/7360208

Research Article

Ultrasonic P-Wave to Acquire Parameters of Boise Sandstone

Guangquan Li, Kui Liu, and Xiang Li

Department of Geophysics, Yunnan University, Kunming, Yunnan 650504, China

Correspondence should be addressed to Guangquan Li; liguangquan@ynu.edu.cn

Received 22 February 2023; Revised 2 May 2023; Accepted 10 July 2023; Published 20 July 2023

Academic Editor: Tianshou Ma

Boise sandstone has a variety of grain diameter, and the heterogeneity makes it difficult to characterize. In this paper, a model of viscous squirt is used to simulate velocity and attenuation of ultrasonic P-wave in the sandstone saturated with water. Phase velocity yielding from the model is fitted against the velocity measured at frequency of 500 kHz, which determinates the quality factor due to viscous squirt (Q_{ps}) as a function of frequency. The resulting Q_{ps} appears to be 14.64 at frequency of 0.8 MHz. With the use of the measured total quality factor (Q_p) of 6.9 at 0.8 MHz, the dry quality factor (Q_{pd}) appears to be 13.0 at 0.8 MHz. The resulting dimension of the rock unit is 0.150 multiplied by 0.140 mm, pretty consistent with the mean grain diameter of 0.150 mm. The relative first and second porosities are ascertained to be 0.976 and 0.024, respectively, and the aperture distance of the second porosity is 0.84 μm. Nonetheless, the model represents analytical continuation of small rock samples. Consequently, seismic attenuation predicted by the model is far smaller than field observation. The discrepancy shows that strong seismic attenuation in the field is associated with a scale much larger than pore scale.

1. Introduction

Rocks in the subsurface contain a variety of pore. Groundwater, oil, or gas may saturate pores. Such rocks are composites consisting of two phases (solid and fluid). In rock physics [1], skeleton (voided solid or dry rock) is more extensively used than solid. In this paper, a rock unit is defined from the Lagrange perspective, which is different from REV (representative elemental volume) defined in the Euler (spatial) sense. The Lagrange approach is tracking of a mass point or an object (which is widely used in theoretical mechanics), i.e., there is no mass into or out of the object. The Euler approach is a field approach (which is widely used in fluid mechanics), i.e., fixing a certain spatial area/volume, and there is mass into or out of the area/volume.

From the perspective of elasticity, fluid flow is free shear dislocation of fluid parcel due to the vanishing shear modulus. From the Lagrange perspective, fluid particles physically migrate long distances. In contrast, although stress waves propagate far away, solid particles just vibrate locally. Undrained rock refers to the extreme case that pore is completely sealed on the boundary of the rock unit (water is not allowed to enter or leave out of the pore). Undrained isotropic rock was firstly studied by [2, 3]. Compressional (P-) wave changes the volume of a rock unit, the volume of pore, and the pressure of fluid [1–6]. For isotropic porous rocks saturated with fluid, shear (S-) wave changes none of the volumes of the rock unit and pore, the fluid pressure, and the shear modulus. Below is the explanation.

According to the invariance of stress tensor [1, 4], for isotropic porous rock, shear stress can be decomposed into a positive pressure (compressional) in one principal direction and a negative pressure (tensional) in the other principal direction with the same magnitude. Suppose that the positive pressure decreases the volumes of the rock unit and pore and increases the pressure of fluid. The negative pressure will increase the volumes of the rock unit and pore and decrease the pressure of fluid. The two effects will cancel each other, resulting in the volumes and fluid pressure unchanged. The above conceptualization is an approximation model with high accuracy and is precisely the basis that Biot [5, 6] constructed his constitutional relations; see equation (2.11) in [5].

Biot [5] used the Darcy permeability to quantify viscous stress between solid and fluid, while Biot [6] used dynamic fluid viscosity (equivalent to dynamic permeability) to quantify the

viscous stress. In view of fluid mechanics, the latter is more reasonable, especially at high frequencies. For S-wave, Biot [6] works pretty well because as aforementioned, shear stress changes none of the volumes of the rock unit and pore and the average fluid pressure within the pore. In short, attenuation of S-wave comes solely from viscous stress between fluid and solid induced by velocity difference between them.

However, the Biot [5, 6] theory severely underestimated the measured velocity and attenuation of ultrasonic P-wave in consolidated rocks [7–9]. More recently, Li et al. [10] demonstrated that the Biot theory worked pretty well for ultrasonic P-wave in unconsolidated glass beads but failed for ultrasonic P-wave in compressed glass beads. Same as any other single-porosity models, the Biot [5, 6] theory is a model in which the average pressure alone is used for a whole pore. There lacks evidence that fluid pressure within a pore is uniform everywhere. Actually, contact of grains (COG) invariably has a volumetric strain much higher than the main pore space (the former is often called as compliant while the latter is called as stiff). As active skeleton compresses passive fluid, COG has a fluid pressure much higher than the main pore space. Consequently, the pressure imbalance drives a viscous squirt between them [11–14], i.e., water mass leaves out of COG and enters the main pore space.

Distinctly different from interpore seepage, viscous squirt is defined as the internal exchange of fluid mass within a pore, in which fluid mass leaves out of a pore space subject to high pressure and enters other space of the pore subject to low pressure. The viscous squirt is characterized by relative shear motion of water with respect to pore wall. Nonetheless, pressure difference may drive fluid to move along with solid, which is not squirt. Take an example. A horizontal glass bottle is fully filled with water. When the bottle has an accelerating translation, there is a pressure difference between its inner bottom (pushing water there) and its inner top (sucking water there). The pressure difference drives the water to achieve the same velocity/acceleration as the bottle, but there are no any squirts within the bottle.

To accurately model viscous squirt between COG and the main pore space, double-permeability model [15–20] was proposed. More recently, an effort of modifying the constitutional relations in [16–18] was made by [21] to automatically yield the Gassmann [2] velocity at the low-frequency end. Later on, the squirt coefficient from mathematical parameterization in [16–18] was upgraded by [22] based on fluid mechanics.

P-wave is associated with pushing/pulling stress onto the surfaces of a rock unit, thus changing the rock-unit volume and the pore pressure [1–6]. Shear stress can be invariably decomposed into a positive pressure (principle stress) on a surface of the Euler element and a negative pressure (principle stress) on another (perpendicular) surface [1, 4, 23]. Recall that S-wave is associated with shear stress on the surfaces of the Euler element. Therefore, S-wave changes neither the rock-unit volume nor the pore volume [1–6] as conceptualized earlier. In [16–18, 24], pore wall close to the boundary of a rock unit was hypothesized to have fluid pressure qualitatively consistent with the principal pressure on the boundary, and it was further hypothesized that the pressure difference drove a squirt within the pore. At high frequencies, there is indeed a pressure difference as depicted in [16, 24]. However, the pressure difference accelerates translation and rotation of pore fluid along with solid, rather than squirt. Fluid mass neither leaves out of a pore space nor enters other space of the pore.

General motions of a solid are comprised of three types, i.e., translation, deformation, and rotation. Theoretical mechanics [25] is focused on study of translation and rotation, while the solid is assumed to be rigid. Elastic mechanics [1, 4, 23] is focused on study of deformation while translation is ignored and rotation plays a negligible role (when wavelength of elastic wave is far longer than length of rock unit).

Similarly, stress waves generally have three effects on rock solid. One effect is accelerating translation of the solid, the second is deformation of the solid, and the third is accelerating rotation of the solid. As pore fluid moves along with the solid, stress waves generally impact the three effects on the fluid. The accelerating translation and rotation of pore fluid require stress difference from pore wall to drive. Whether for P-wave or for S-wave, pore fluid has accelerating translation, deformation, and accelerating rotation. Deformation can be further classified as bulk deformation and shear deformation [1, 4, 23]. For bulk deformation of pore fluid, P-wave changes the pore volume and fluid pressure. However, it is controversial whether S-wave changes the pore volume and fluid pressure [16–18] or not [5, 6, 26–29].

Fluid is characterized with a vanishing shear modulus which does not allow any elastic shear stress. As such, shear deformation of pore fluid is associated with viscous shear stress in fluid mechanics. According to theorem of angular momentum [25], at exceptionally high frequency, accelerating rotation of pore fluid requires stress difference from pore wall to drive. For P-wave, accelerating translation and shear deformation of pore fluid are driven by pressure difference (see the above example of a horizontal glass bottle saturated with water) and/or viscous shear stress from pore wall. For S-wave, accelerating translation and shear deformation of pore fluid are driven by viscous shear stress [26, 27] and/or pressure difference from pore wall [28, 29].

Based upon the intrapore squirt, Li et al. [21] and Li [22] developed a model of P-wave in isotropic rock saturated with fluid. For Berea sandstone (a classic sandstone with relatively uniform diameter of grain), the model [21, 22] accurately simulated ultrasonically measured velocity and attenuation [30] of the sandstone saturated with water.

Different from Berea sandstone, Boise sandstone has a wide distribution of grain diameter and is highly heterogeneous at the grain scale. As such, Boise sandstone is more difficult to describe than Berea sandstone, and its parameters vary appreciably from specimen to specimen. Nevertheless, Boise sandstone may be conceptualized to be statistically homogenous on a macroscopic scale, i.e., tens of grain diameter. Wave approach is advantageous and promising in acquiring the average parameters, because stress wave transmits through a rock sample with a dimension of several centimeters. King [31] well measured velocity of ultrasonic

P-wave in Boise sandstone both dry and saturated. In this paper, the squirt model [21, 22] shall be used to simulate the saturated velocity and to predict the viscous squirt attenuation of Boise sandstone in [31]. The motivation is to confirm the applicability of the model [21, 22] to Boise sandstone and to acquire its average parameters.

2. Model of P-Wave

Viscous squirt between COG and the main pore space can be assumed to be in a 2D fissure [22]. Hence, squirt coefficient, $\gamma(\omega)$, was derived as follows [22, 32]:

$$\gamma(\omega) = \frac{8i\eta_2}{\omega\rho_f L^2}\left(\frac{\tanh\varphi}{\varphi} - 1\right), \tag{1}$$

with

$$\varphi = \sqrt{\frac{\omega}{2\nu}}(1+i)\frac{b}{2}, \tag{2}$$

where η_2 is the second porosity, ω is the angular frequency ($f = \omega/2\pi$ is the wave frequency), ρ_f is the fluid density, $\nu = \mu/\rho_f$ is the fluid kinematic viscosity (μ is the fluid dynamic viscosity), b is the aperture distance of COG, and L and D are the length and depth of the rock unit, respectively. Please note that $\eta_2 = b/D$.

Albeit permeability is important for slow P-wave (transmission of the fluid pressure which drive groundwater seepage in hydrogeology) [33, 34], it can be well ignored as the first-order approximation in the study of fast P-wave at high frequencies [21, 22]. The reason is that viscous squirt within a pore (rather than interpore permeability) dominates attenuation of fast P-wave at high frequencies. This led to the wavenumber (k) equation as follows [21, 22]:

$$\left(\frac{k}{\omega}\right)^2\left(\frac{4}{3}Gs_1 + \frac{4}{3}Gs_2 + \left(K_d + \frac{4}{3}G\right)s_3\right) = \rho(s_1 + s_2 + s_3), \tag{3}$$

where K_d and G are the bulk modulus and shear modulus of skeleton, respectively, $\rho = \rho_s + \eta\rho_f$ is the total density, and

$$s_1 = \frac{1}{a_{13}}\left[\left(\eta_2 a_{13} - a_{33} - \frac{\gamma(\omega)}{\omega i}\right)(\eta_1 a_{11} - a_{21}) - \left(\eta_1 a_{13} + \frac{\gamma(\omega)}{\omega i}\right)(\eta_2 a_{11} - a_{31})\right],$$

$$s_3 = \frac{a_{11}}{a_{12}a_{13}}\left[\eta_1\eta_2 a_{12}a_{13} - (\eta_1 a_{12} - a_{22})(\eta_2 a_{13} - a_{33}) + \frac{\gamma(\omega)}{\omega i}(\eta a_{12} + \eta a_{13} - a_{22} - a_{33})\right]$$

$$s_3 = \frac{a_{11}}{a_{12}a_{13}}\left[\eta_1\eta_2 a_{12}a_{13} - (\eta_1 a_{12} - a_{22})(\eta_2 a_{13} - a_{33}) + \frac{\gamma(\omega)}{\omega i}(\eta a_{12} + \eta a_{13} - a_{22} - a_{33})\right], \tag{4}$$

wherein η_1 is the first porosity and a_{ij} is the unsymmetric compressibility matrices [21, 22].

Wavenumber equation (3) was rewritten as follows for simplicity:

$$(-b_1 + b_2 i)\left(\frac{k}{\omega}\right)^2 = -c_1 + c_2 i, \tag{5}$$

where $-b_1$ and b_2 are the real part and imaginary part of $(4/3)Gs_1 + (4/3)Gs_2 + (K_d + (4/3)G)s_3$, respectively, while $-c_1$ and c_2 are the real part and imaginary part of $\rho(s_1 + s_2 + s_3)$, respectively.

Equation (5) has the solution as follows [22, 35]:

$$\sqrt{b_1^2 + b_2^2}\left(\frac{k}{\omega}\right) = A_1 + A_2 i = \left[\frac{(c_1b_1 + c_2b_2) + \sqrt{(c_1b_1 + c_2b_2)^2 + (c_1b_2 - b_1c_2)^2}}{2}\right]^{1/2} - i\left[\frac{-(c_1b_1 + c_2b_2) + \sqrt{(c_1b_1 + c_2b_2)^2 + (c_1b_2 - b_1c_2)^2}}{2}\right]^{1/2}, \tag{6}$$

wherein A_1 and A_2 are the two buffer real numbers.

Hence, phase velocity (v_p) and the quality factor (Q_{ps}) due to viscous squirt turned out to be as follows [21, 22]:

$$v_p = \frac{\sqrt{b_1^2 + b_2^2}}{A_1}, \qquad Q_{ps} = \frac{-A_1}{2A_2}. \tag{7}$$

3. Application to Boise Sandstone

Forming during the Tertiary period and outcropping in Boise City, Idaho, in the USA, Boise sandstone is highly porous and highly permeable. The specimen had a porosity of 0.25 [31], the solid material had a density of 2650 kg/m^3 [36], and the dry specimen had a density of 1988 kg/m^3. Dry velocities of P- and S-waves under differential pressure of 3 MPa were measured as 3070 and 1960 m/s, respectively [31]. Thus, bulk (K_d) and shear (G) modules are calculated as 8.55 and 7.64 GPa, respectively. The P-wave had frequency of 500 kHz [31], and measured parameters are listed in Table 1.

The velocity of P-wave in the water-saturated specimen was measured as 3300 m/s [31], under differential pressure of 3 MPa. As attenuation was not measured in [31], we have

Table 1: Measured parameters of Boise sandstone and water.

Parameters	Values	Units	References
Density of skeleton (ρ_s)	1988	kg·m^{-3}	[31]
Bulk compressibility (β_d)	0.117×10^{-9}	Pa^{-1}	[31]
Compressibility of solid material (β_s)	0.027×10^{-9}	Pa^{-1}	[36]
Shear modulus (G)	7.64×10^{9}	Pa	[31]
Porosity (η)	0.25		[31]
Density of water (ρ_f)	1000	kg·m^{-3}	[37]
Viscosity of water (μ)	0.001	Pa·s	[37]
Compressibility of water (β_f)	0.46×10^{-9}	Pa^{-1}	[38]

Table 2: Porosities, compressibility matrices, and length scales in modeling Boise sandstone. COG denotes contact of grains.

Parameters	Values	Units
First porosity (η_1)	0.976η	
Second porosity (η_2)	0.024η	
Skeleton strain divided by main pore pressure (a_{12})	$(\beta_s - \beta_d)\eta 1/\eta$	Pa^{-1}
Skeleton strain divided by COG pressure (a_{13})	$(\beta_s - \beta_d)\eta 2/\eta$	Pa^{-1}
Fluid increase in main pore divided by COG pressure (a_{23})	0	Pa^{-1}
Fluid increase in COG divided by main pore pressure (a_{32})	0	Pa^{-1}
Fluid increase in main pore divided by main pore pressure (a_{22})	0.70 ($\eta\beta_f + \beta_P$)	Pa^{-1}
Fluid increase in COG divided by COG pressure (a_{33})	0.30 ($\eta\beta_f + \beta_P$)	Pa^{-1}
Fluid increase in main pore divided by confining pressure (a_{21})	$\beta_C\eta 1/\eta$	Pa^{-1}
Fluid increase in COG divided by confining pressure (a_{31})	$\beta_C\eta 2/\eta$	Pa^{-1}
Aperture distance of COG (b)	0.84	μm
Length of rock unit (L)	150	μm
Depth of rock unit (D)	140	μm

to use the total quality factor (Q_p of 6.9 at 0.8 MHz) documented in [30]. The specimen in [30] had the same porosity as in [31], whereas the former had v_p of 3420 m/s, a little higher than the latter of 3300 m/s. The modeling target is that both phase velocity and the quality factor are close between the model and the measurement. Modeling parameters are collected in Table 2.

In the modeling, the key parameters are the second porosity (η_2), the aperture distance of COG (b), and the rock-unit length (L). The first porosity can be automatically determined via $\eta_1 = \eta - \eta_2$, and the rock-unit depth can be automatically determined via $D = b/\eta_2$. Our model yields v_p and Q_s as depicted in Figures 1 and 2, respectively. At low frequencies, modeled v_p asymptotes to Gassmann [2] velocity of 3228 m/s. The model yields v_p of 3301 m/s at frequency of 0.5 MHz and Q_{ps} of 14.64 at frequency of 0.8 MHz. Dry quality factor (Q_{pd}) is thus calculated as 13.0, via the following relation [1]:

$$\frac{1}{Q_{pd}} = \frac{1}{Q_p} - \frac{1}{Q_{ps}}. \quad (8)$$

Please note that in this paper, attenuation due to the Rayleigh scattering is incorporated into dry attenuation on the left hand side of equation (8). In other words, we do not discern attenuation due to the Rayleigh scattering from dry attenuation. L and D of the rock unit turn out to be 150 and 140 μm, respectively. According to [39], Boise sandstone has grain diameter ranging from 75 to 225 μm (150 μm on average).

Squirt flux rate from COG to the main pore space is squirt coefficient, $\gamma(\omega)$, multiplied by pressure difference between them. The modeling also yields $\gamma(\omega)$ as a function of frequency; see Figure 3. Evidently, with frequency lower than 0.1 MHz, $\gamma(\omega)$ is nearly a real-number constant, meaning that the squirt flux rate is almost synchronous with the pressure difference. With the increase of frequency, $\gamma(\omega)$ becomes a complex number, meaning that the squirt flux rate is less synchronous with the pressure difference. With the further increase of frequency from 10 MHz, $\gamma(\omega)$ will asymptote to zero, meaning a vanishing squirt flux rate.

4. Discussion

Gregory [36] also measured velocity of ultrasonic P-wave in Boise sandstone. The specimen of Boise sandstone in [36]

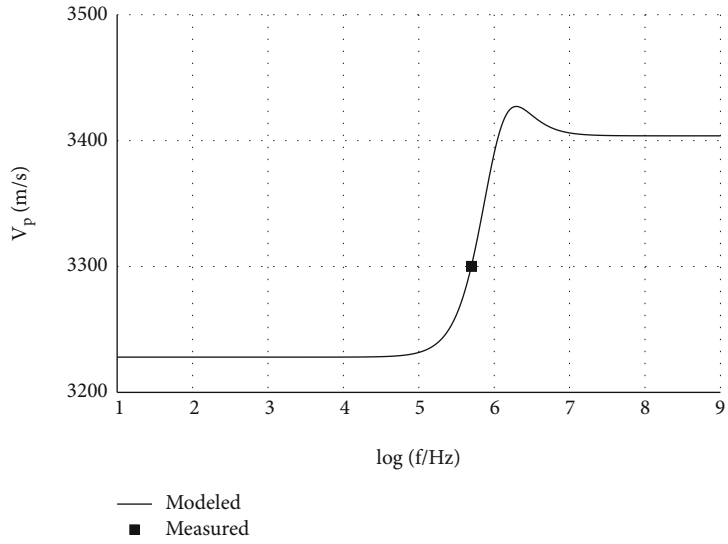

Figure 1: Modeled velocity (v_p) versus ultrasonic measurement [31] of P-wave in Boise sandstone, with f denoting frequency and modeling parameters from Table 2.

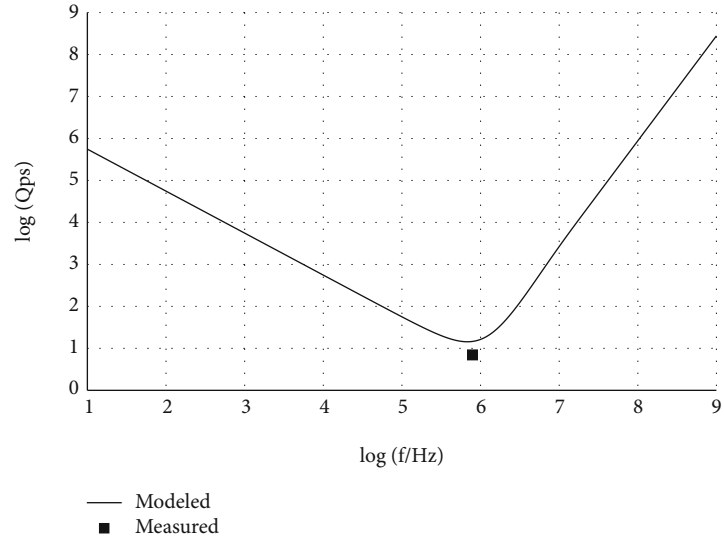

Figure 2: Modeled quality factor of P-wave due to viscous squirt (Q_{ps}) versus the total quality factor (Q_p) [30] measured on Boise sandstone, with f denoting frequency and modeling parameters from Table 2.

had a porosity of 0.268 (which is higher than the porosity in [31]) and a dry density of 1940 kg/m^3. Dry velocities of P- and S-waves were measured as 3290 and 2090 m/s, respectively [36]; both were higher than the counterparts in [31]. v_p (at frequency of 1 MHz) was measured as 3455 m/s in [36], appreciably higher than v_p of 3300 m/s (at frequency of 500 kHz) measured in [31].

In the previous study [22], the same model as in this paper was used for simulating v_p measured on the specimen in [36]; the modeling parameters are listed in Table 3 in [22]. The aperture distance of COG (b) was 1.0 μm in [22] and is 0.84 μm in this paper. In the modeling of Li [22], L and D of the rock unit were 145 and 149 μm, respectively, while in this paper, L and D are 150 and 140 μm, respectively.

For Boise sandstone having a porosity of 0.25, Q_{ps} was predicted as 16.1 at frequency of 0.8 MHz [22], while Q_{ps} is predicted as 14.64 in this paper. The small error in Q_{ps} may arise from the different specimens and the different confining pressures. Via equation (8), Q_{pd} in [22] appeared to be 12.1 at 0.8 MHz, while Q_{pd} in this study turns out to be 13.0 at the frequency. The error in Q_{pd} is also small. On the other hand, for Berea sandstone having a porosity of 0.20, Q_{pd} under zero confining pressure was measured as approximately 20 at frequency of 0.8 MHz [30]. The increasing porosity tends to decrease Q_{pd} and enhance dry attenuation. The total quality factor (Q_p) was measured as 6.9 for water-saturated Boise sandstone and as approximately 10

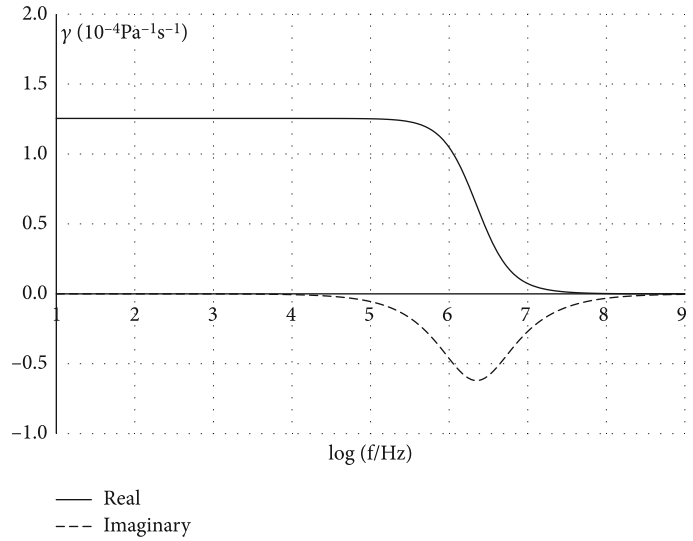

Figure 3: Squirt coefficient $\gamma(\omega)$ for water-saturated Boise sandstone, with f denoting frequency. Please note that at very high frequencies, the coefficient tends to vanish according to equations (1) and (2).

Table 3: Porosities, compressibility matrices, and length scales in modeling Boise sandstone. COG denotes contact of grains.

Parameters	Values	Units
First porosity (η_1)	0.985η	
Second porosity (η_2)	0.015η	
Skeleton strain divided by main pore pressure (a_{12})	$(\beta_s - \beta_d)\eta 1/\eta$	Pa^{-1}
Skeleton strain divided by COG pressure (a_{13})	$(\beta_s - \beta_d)\eta 2/\eta$	Pa^{-1}
Fluid increase in main pore divided by COG pressure (a_{23})	0	Pa^{-1}
Fluid increase in COG divided by main pore pressure (a_{32})	0	Pa^{-1}
Fluid increase in main pore divided by main pore pressure (a_{22})	$0.85\left(\eta\beta_f + \beta_P\right)$	Pa^{-1}
Fluid increase in COG divided by COG pressure (a_{33})	$0.15\left(\eta\beta_f + \beta_P\right)$	Pa^{-1}
Fluid increase in main pore divided by confining pressure (a_{21})	$\beta_C\eta 1/\eta$	Pa^{-1}
Fluid increase in COG divided by confining pressure (a_{31})	$\beta_C\eta 2/\eta$	Pa^{-1}
Aperture distance of COG (b)	0.5	μm
Length of rock unit (L)	150	μm
Depth of rock unit (D)	133	μm

for water-saturated Berea sandstone [30]. A higher porosity inclines to decrease Q_p and enlarge the total attenuation.

As depicted in Figure 1, the dispersion curve is characterized with a small concave at 1 MHz. The concave is very interesting and was rarely observed previously. To confirm the concave, we purposely change the modeling parameters from Table 2 into Table 3. Then, the model output is plotted in Figures 4 and 5. It is seen in Figure 4 that although the dispersion curve is almost monotonous, the measured velocity is not well simulated. In Figure 5, the disparity of the quality factor between model and measurement is very large. Therefore, the concave in Figure 1 is a must yielding from the accurate fitting between model and measurement.

At the first glance, Figures 1 and 2 have only measurements at a single frequency (500 kHz). Nonetheless, there is another implicit frequency in seismic band (10-100 Hz). In the seismic band, the model yields the classic Gassmann [2] velocity of 3228 m/s and a high-quality factor of 10^5, which is consistent with the consensus that at seismic frequencies, P-wave in a rock will approach the elastic limit. For sonic frequencies (20 Hz to 20 kHz), the current technique of a resonant bar is not quite reliable and not widely used. At laboratories, few people conducted sonic measurements with transient waves, which would require a very large specimen.

The low-frequency end in Figures 1 and 2 represents analytical continuation of the small specimen to a very large scale. Along this line, our model predicts Q_{ps} as 10^6 with frequency at 10 Hz. However, according to the measurement by seismic P-wave in the southern California crust [40], seismic

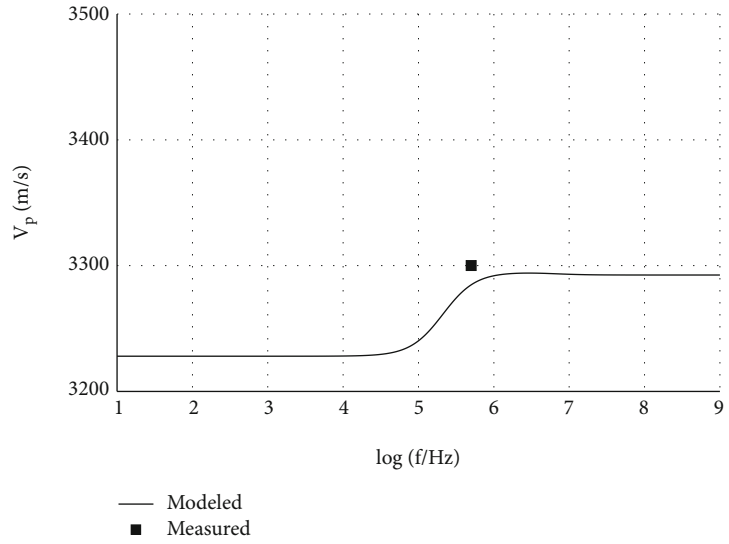

Figure 4: Modeled velocity (v_p) versus ultrasonic measurement [31] of P-wave in Boise sandstone, with f denoting frequency and modeling parameters from Table 3.

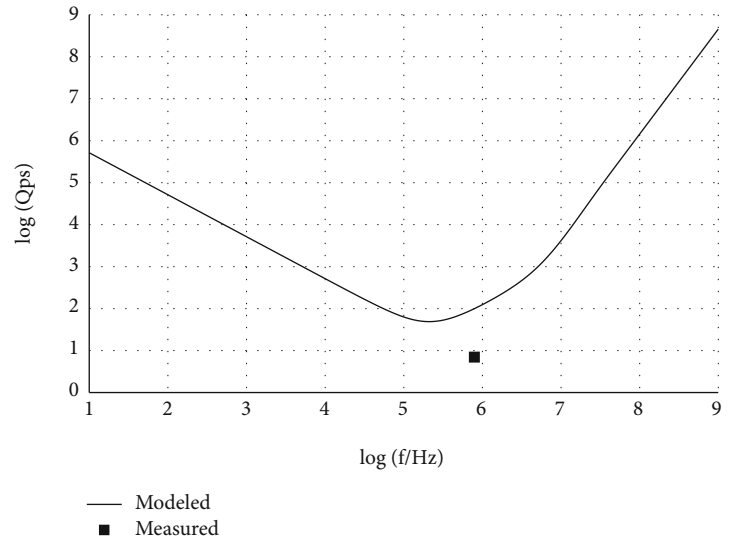

Figure 5: Modeled quality factor of P-wave due to viscous squirt (Q_{ps}) versus the total quality factor (Q_p) [30] measured on Boise sandstone, with f denoting frequency and modeling parameters from Table 3.

Q_p ranged from 100 to 200 at an aquifer depth of 1 km. The large disparity robustly shows that the intrapore squirt is not the mechanism of seismic attenuation in the field. Instead, severe seismic attenuation in the field probably arises from the scaling effect. Recall that measurements of Q_p are based upon direct wave. Large faults broke the crust, thus tending to decrease velocity of direct wave and increase attenuation of direct wave. Geologic blocks are likely to cause wave reflections between them and the Rayleigh scattering (as manifested by coda wave), thus decreasing the amplitude of direct wave. Multiple lithological layers also cause multiple reflections which can decrease amplitude of direct wave and elongate waveform [41]. All these can increase apparent attenuation in the field.

5. Conclusions

(1) Although Boise sandstone has a wide distribution of grain diameter, our model of intrapore squirt well simulates both velocity and attenuation of P-wave ultrasonically measured. This shows that the wave approach is capable of acquiring the macroscopic parameters because the wave scans throughout the sandstone. The reason is that at frequency of 500 kHz, the wavelength is 6.6 mm which is far longer than the maximum grain diameter of 0.225 mm

(2) The resulting dimension of the rock unit is 0.150 multiplied by 0.140 mm, pretty consistent with the

mean grain diameter of 0.150 mm. The relative first and second porosities are 0.976 and 0.024, respectively, and the aperture distance of COG is 0.84 μm

(3) In the previous study [22], Q_{ps} was predicted as 16.1 at frequency of 0.8 MHz, while it is predicted as 14.64 at the frequency by this study. These two values are close to each other, and the small error may arise from the different specimens and the different confining pressures

(4) At frequency of 0.8 MHz, Q_{pd} appears to be 13.0 for Boise sandstone having a porosity of 0.25, while Q_{pd} was measured as approximately 20 for the dry Berea sandstone having a porosity of 0.20. Increase of porosity tends to enlarge dry attenuation and decrease Q_{pd}

Nomenclature

a_{ij}: Compressibility matrices
b: Aperture distance of COG
D: Depth of the rock unit
f: Frequency
G: Shear modulus of dry rock
k: Wavenumber
L: Length of the rock unit
K_d: Bulk modulus of dry rock
Q_p: The total quality factor of P-wave
Q_{pd}: The quality factor of P-wave in dry rock
Q_{ps}: The quality factor of P-wave due to viscous squirt
v_p: Phase velocity of P-wave
β_d: Bulk compressibility of dry rock ($\beta_d = 1/K_d$)
β_f: Bulk compressibility of fluid
β_p: Change of porosity due to fluid pressure
β_C: Change of porosity due to the confining pressure
β_s: Compressibility of solid material
μ: Fluid dynamic viscosity
ν: Fluid kinematic viscosity ($\nu = \mu/\rho_f$)
ρ: The total density
ρ_f: Fluid density
ρ_s: Skeleton density
φ: Permeability angle
η: Rock porosity
η_1: The first porosity
η_2: The second porosity
ω: Angular frequency
γ: Squirt coefficient.

Data Availability

The data of this study are included within the article.

Additional Points

Highlights. A squirt model of P-wave is used to acquire the average parameters of Boise sandstone. (1) At frequency of 0.8 MHz, the quality factors under dry and viscous squirt conditions are 13.0 and 14.64, respectively. (2) Increase of porosity tends to enlarge dry attenuation of P-wave and decrease dry quality factor.

Conflicts of Interest

The authors declare that they have no conflicts of interest.

Acknowledgments

The study was sponsored by the National Natural Science Foundation of China under grant 42064006.

References

[1] J. Jaeger, N. Cook, and R. Zimmerman, *Fundamentals of Rock Mechanics*, Wiley-Blackwell, fourth ed edition, 2007.

[2] F. Gassmann, "Uber die Elasticität Poröser Medien [On the elasticity of porous media]," *Vierteljahrsschrift der Naturforschenden Gesllschaft in Zürich*, vol. 96, pp. 1–23, 1951.

[3] A. W. Skempton, "The pore-pressure coefficients A and B," *Geotechnique*, vol. 4, no. 4, pp. 143–147, 1954.

[4] A. Green and W. Zerna, *Theoretical Elasticity*, Oxford University Press, 1954.

[5] M. A. Biot, "Theory of propagation of elastic waves in a fluid-saturated porous solid. I. Low-frequency range," *Journal of the Acoustic Society of America*, vol. 28, no. 2, pp. 168–178, 1956.

[6] M. A. Biot, "Theory of propagation of elastic waves in a fluid-saturated porous solid. II. Higher frequency range," *Journal of the Acoustic Society of America*, vol. 28, no. 2, pp. 179–191, 1956.

[7] R. J. O'Connell and B. Budiansky, "Viscoelastic properties of fluid-saturated cracked solids," *Journal of Geophysical Research*, vol. 82, pp. 5719–5735, 1977.

[8] S. Mochizuki, "Attenuation in partially saturated rocks," *Journal of Geophysical Research*, vol. 87, pp. 8598–8604, 1982.

[9] T. Jones and A. Nur, "Velocity and attenuation in sandstone at elevated temperatures and pressures," *Geophysical Research Letters*, vol. 10, no. 2, pp. 140–143, 1983.

[10] G. Li, Y. Wang, and X. Li, "Minor squirt in unconsolidated sands versus strong squirt in compressed glass beads," *Geofluids*, vol. 2020, Article ID 8486154, 8 pages, 2020.

[11] G. Mavko and A. Nur, "Melt squirt in the asthenosphere," *Journal of Geophysical Research*, vol. 80, no. 11, pp. 1444–1448, 1975.

[12] J. Dvorkin and A. Nur, "Dynamic poroelasticity: a unified model with the squirt and the Biot mechanisms," *Geophysics*, vol. 58, pp. 524–533, 1993.

[13] W. Murphy, K. Winkler, and R. Kleinberg, "Frame modulus reduction in sedimentary rocks: the effect of adsorption on grain contacts," *Geophysical Research Letters*, vol. 11, no. 9, pp. 805–808, 1984.

[14] W. Murphy, K. Winkler, and R. Kleinberg, "Acoustic relaxation in sedimentary rocks: dependence on grain contacts and fluid saturation," *Geophysics*, vol. 51, no. 3, pp. 757–766, 1986.

[15] J. Berryman and F. Wang, "The elastic coefficients of double-porosity models for fluid transport in jointed rock," *Journal of Geophysical Research*, vol. 100, no. B12, pp. 24611–24627, 1995.

[16] S. R. Pride and J. G. Berryman, "Linear dynamics of double-porosity dual-permeability materials. I. Governing equations

and acoustic attenuation," *Physical Review E*, vol. 68, no. 3, 2003.

[17] S. R. Pride and J. G. Berryman, "Linear dynamics of double-porosity dual-permeability materials: II. Fluid transport equations," *Physical Review E*, vol. 68, article 036604, 2003.

[18] S. R. Pride, J. G. Berryman, and J. M. Harris, "Seismic attenuation due to wave-induced flow," *Journal of Geophysical Research*, vol. 109, no. B1, 2004.

[19] J. Auriault, C. Boutin, and C. Geindreau, *Homogenization of Coupled Phenomena in Heterogeneous Media*, John Wiley & Sons, 2009.

[20] C. Boutin and P. Royer, "On models of double porosity poroelastic media," *Geophysical Journal International*, vol. 203, no. 3, pp. 1694–1725, 2015.

[21] G. Li, Y. Mu, and C. Xie, "Unsymmetric compressibility matrix to model P-wave attenuation," *Acta Geodaetica et Geophysica*, vol. 56, no. 3, pp. 407–424, 2021.

[22] G. Li, "A new squirt coefficient to simulate P-wave attenuation," *Geophysical Prospecting*, vol. 70, no. 4, pp. 815–827, 2022.

[23] Q. Du, S. Yu, and Z. Yao, *Elasticity Theory*, The Science Press of China, 1986.

[24] J. Dvorkin, G. Mavko, and A. Nur, "Squirt flow in fully saturated rocks," *Geophysics*, vol. 60, no. 1, pp. 97–107, 1995.

[25] A. Fetter and J. Walecka, *Theoretical Mechanics of Particles and Continua*, McGraw-Hill, 1980.

[26] G. Li, "S wave attenuation based on Stokes boundary layer," *Geophysical Prospecting*, vol. 68, pp. 910–917, 2020.

[27] G. Li and C. Xie, "Calculation of matrix permeability from velocity and attenuation of ultrasonic S-wave," *Journal of Geophysics and Engineering*, vol. 18, no. 6, pp. 984–994, 2021.

[28] G. Li, Y. Liu, and S. Liu, "S-wave attenuation due to fluid acceleration," *Pure and Applied Geophysics*, vol. 179, no. 4, pp. 1159–1172, 2022.

[29] G. Li, H. Zhao, Q. Wang, Z. Wang, and H. Luo, "The mechanisms of S-wave attenuation in grainstones," *Journal of Geophysics and Engineering*, vol. 19, no. 5, pp. 997–1004, 2022.

[30] M. Toksöz, D. Johnston, and A. Timur, "Attenuation of seismic waves in dry and saturated rocks: I. Laboratory measurements," *Geophysics*, vol. 44, no. 4, pp. 681–690, 1979.

[31] M. S. King, "Wave velocities in rocks as a function of changes in overburden pressure and pore fluid saturants," *Geophysics*, vol. 31, no. 1, pp. 50–73, 1966.

[32] H. Schlichting, *Boundary Layer Theory, Sixth Ed*, Springer, 1968.

[33] G. Li, K. Liu, and X. Li, "Comparison of fluid pressure wave between Biot theory and storativity equation," *Geofluids*, vol. 2020, Article ID 8820296, 8 pages, 2020.

[34] G. Li, Y. Miao, and Y. Mei, "Monochromatic wave of fluid pressure in a porous rock," *Ground Water*, vol. 61, no. 4, pp. 544–551, 2023.

[35] M. J. Ablowitz and A. S. Fokas, *Complex Variables: Introduction and Applications*, Cambridge University Press, New York, 1997.

[36] A. R. Gregory, "Fluid saturation effects on dynamic elastic properties of sedimentary rocks," *Geophysics*, vol. 41, no. 5, pp. 895–921, 1976.

[37] P. K. Kundu, *Fluid Mechanics*, Academic Press, San Diego, 1990.

[38] R. A. Fine and F. J. Millero, "Compressibility of water as a function of temperature and pressure," *Journal of Chemical Physics*, vol. 59, no. 10, pp. 5529–5536, 1973.

[39] C. S. Cheung, P. Baud, and T. Wong, "Effect of grain size distribution on the development of compaction localization in porous sandstone," *Geophysical Research Letters*, vol. 39, no. 21, article L21302, 2012.

[40] E. Hauksson and P. M. Shearer, "Attenuation models (Q_P and Q_S) in three dimensions of the southern California crust: inferred fluid saturation at seismogenic depths," *Journal of Geophysical Research*, vol. 111, no. B5, article B05302, 2006.

[41] K. H. Waters, *Reflection Seismology–A Tool for Energy Resource Exploration*, Wiley, New York, 1981.